

Proceeding Series of the Brazilian Society of Computational and Applied Mathematics

Space Debris: Reentry and Collision Risk

Jarbas Cordeiro Sampaio¹

Departamento de Ensino IFBA, Camacari, BA

Ewerton Felipe B. P. dos Santos²

Departamento de Ensino IFBA, Camacari, BA

Abstract. The increasing number of uncontrolled objects orbiting the Earth justifies efforts to observe and track them in order to avoid collisions among them and operational artificial satellites. These studies involve different disturbances and resonances in the orbital motion of these objects. Most of the cataloged space debris are found in low earth orbits (LEO). This work studies the orbital motion of space debris around the Planet. Real data from the 2-line element set provided by NORAD (North American Defense) are used to compare with the results obtained for orbital motions. The geopotential and atmospheric drag are used as perturbations in the SGP4 model. Figures show the time behavior of the orbital elements of the space debris in the process of reentry in the Earth. Solutions for the space debris mitigation are necessary.

Key Words. Space Debris, Reentry, Collision Risk.

1 Introduction

Since the launch of the first satellite, several space missions have been realized putting objects around the Earth. In this way, several studies are important to preserve the operability and integrity of the operational artificial satellites, considering the increasing number of distinct objects in the space environment offering collision risks and, consequently, possible lost of mission [2].

The orbital dynamics of cataloged objects can be analyzed using the 2-line element group, or TLE of the NORAD (North American Defense). The TLE data are composed of seven parameters and epoch [1, 5].

Figure 1 shows that most of objects are in the region $13 < n \text{ (rev/day)} < 15$ by the histogram of the mean motion of artificial satellites and space debris in LEO region.

Synchronous satellites in circular or elliptical orbits have been extensively studied in the literature, due to the study of resonant orbits characterizing the dynamics of these objects [3, 4].

In this work, a study is done about objects with orbital motions around the Earth in LEO region. These space debris reentry in the Planet in some moment. The TLE data

¹jarbassampaio@ifba.edu.br

²es.santos.felipe@gmail.com

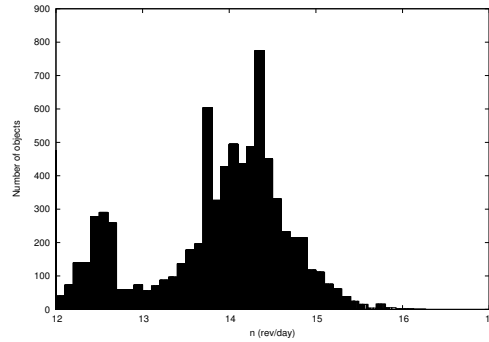


Figure 1: Histogram of the mean motion of the cataloged objects in LEO region.

of the cataloged objects are used and the orbit propagation is done considering the effects of the Geopotential and Atmospheric Drag. Solutions for the space debris mitigation are necessary.

In the next section, a propagation of the orbit is presented showing solutions for the time behavior of the orbital elements.

2 Propagation of the orbit

In this section, a method used to propagated the orbit is described. The initial data of the space debris are taken from the real orbital motions shown in the Two-Line Elements described before (see Figure 1). First, the real data are corrected and then propagated in time using the SGP4 model. More details about this method is shown in [1]. The SGP model was used by the National Space Surveillance Control Center and after by the United States Space Surveillance Network with the goal to track the objects in orbital motions.

A previous study, described in [3], shows a large research in resonant regions with several objects, including space debris. Results show that most of objects are in the region $13 < n < 16$, where n is the mean motion. The International Space Station is in the related region and studies about proximities with space debris, safety orbits and collision risks are natural consequences of the development of the work.

The propagation method shown in the present work considers effects of the geopotential and atmospheric drag, see Eqs. 7 to 19, while previous works, see [3] and [4], they consider only corrections in the TLE data and effects of the geopotential in the orbital dynamics of space debris shown by Eqs. 1 to 6.

The corrections in TLE data shown by Eqs. 1 to 6 are necessary because the Earth's atmosphere cause differences in the data produced by the sensors. Considering n_1 the mean motion of the 2-line, the semi-major axis a_1 is calculated by Eq. (1).

$$a_1 = \left(\frac{\sqrt{\mu}}{n_1} \right)^{2/3} \quad (1)$$

where μ is the Earth gravitational parameter, $\mu=3.986009 \times 10^{14} \text{ m}^3/\text{s}^2$. Using a_1 , the

parameter δ_1 is calculated by Eq. (2) .

$$\delta_1 = \frac{3}{4} J_2 \frac{a_e^2}{a_1^2} \frac{(3\cos^2(I) - 1)}{(1 - e^2)^{3/2}}, \quad (2)$$

where a_e is the Earth mean equatorial radius, $a_e=6378.135 \text{ km}$, J_2 is the second zonal harmonic, $J_2 = 1,0826 \times 10^{-3}$, e is the eccentricity and I is the inclination of the orbital plane with the equator.

Now, the new semi-major axis a_o is defined using δ_1 , from Eq. (2) [1].

$$a_o = a_1 \left[1 - \frac{1}{3}\delta_1 - \delta_1^2 - \frac{134}{81}\delta_1^3 \right], \quad (3)$$

and a new mean motion n'_o and semi-major axis a'_o are found by the parameter δ_o

$$\delta_o = \frac{3}{4} J_2 \frac{a_e^2}{a_o^2} \frac{(3\cos^2(I) - 1)}{(1 - e^2)^{3/2}}, \quad (4)$$

$$n'_o = \frac{n_1}{1 + \delta_o}, \quad (5)$$

$$a'_o = \frac{a_o}{1 - \delta_o}. \quad (6)$$

The secular effects of gravitation and atmospheric drag are included in the next equations.

$$M' = M + \left[1 + \frac{3J_2 a_e^2 (-1 + 3\theta^2)}{4a_o'^2 \beta^3} + \frac{3J_2^2 a_e^4 (13 - 78\theta^2 + 137\theta^4)}{64a_o'^4 \beta^7} \right] n'_o (t - t_o), \quad (7)$$

$$\begin{aligned} \omega' = \omega + & \left[-\frac{3J_2 a_e^2 (1 - 5\theta^2)}{4a_o'^2 \beta^4} + \frac{3J_2^2 a_e^4 (7 - 114\theta^2 + 395\theta^4)}{64a_o'^4 \beta^8} \right. \\ & \left. - \frac{15J_4 a_e^4 (3 - 36\theta^2 + 49\theta^4)}{32a_o'^4 \beta^8} \right] n'_o (t - t_o), \end{aligned} \quad (8)$$

$$\Omega' = \Omega + \left[-\frac{3J_2 a_e^2 \theta}{2a_o'^2 \beta^4} + \frac{3J_2^2 a_e^4 (4\theta - 19\theta^3)}{8a_o'^4 \beta^8} - \frac{15J_4 a_e^4 \theta (3 - 7\theta^2)}{16a_o'^4 \beta^8} \right] n'_o (t - t_o), \quad (9)$$

$$\delta\omega' = B^* C_3(\cos(\omega))(t - t_o), \quad (10)$$

$$\delta M' = -\frac{2}{3}(q_o - \epsilon)^4 B^* \varrho^4 \frac{a_e}{e\eta} [(1 + \eta \cos(M'))^3 - (1 + \eta \cos(M))^3], \quad (11)$$

$$M'' = M' + \delta\omega' + \delta M', \quad (12)$$

$$\omega'' = \omega' - \delta\omega' - \delta M', \quad (13)$$

$$\Omega'' = \Omega' - \frac{21}{4} \frac{n'_o J_2 a_e^2 \theta}{a_o'^2 \beta^2} C_1 (t - t_o)^2, \quad (14)$$

$$e'' = e - B^* C_4 (t - t_o) - B^* C_5 (\sin(M'') - \sin(M)), \quad (15)$$

$$a'' = a'_o [1 - C_1 (t - t_o) - D_2 (t - t_o)^2 - D_3 (t - t_o)^3 - D_4 (t - t_o)^4]^2, \quad (16)$$

$$\begin{aligned} \kappa'' = & M'' + \omega'' + \Omega'' + n'_o \left[\frac{3}{2} C_1 (t - t_o)^2 + (D_2 + 2C_1^2) (t - t_o)^3 \right. \\ & + \frac{1}{4} (3D_3 + 12C_1 D_2 + 10C_1^3) (t - t_o)^4 \\ & \left. + \frac{1}{5} (3D_4 + 12C_1 D_3 + 6D_2^2 + 30C_1^2 D_2 + 15C_1^4) (t - t_o)^5 \right], \quad (17) \end{aligned}$$

$$\beta'' = \sqrt{1 - e''^2}, \quad (18)$$

$$n'' = \sqrt{\frac{\mu}{a''^3}}, \quad (19)$$

where ω is the argument of pericentre, Ω is the longitude of the ascending node and M is the mean anomaly. $(t - t_o)$ is the time since epoch, B^* is the drag coefficient and J_4 the fourth gravitational zonal harmonic of the Earth.

Observe that Eqs. 7 to 19 show transformations, $(a, e, \omega, \Omega, M) \rightarrow (a'', e'', \omega'', \Omega'', M'')$, in the classical orbital elements and in other variables, as mean motion n . These transformations represent corrections in TLE data and effects of geopotential and atmospheric drag are included in orbital motions of space debris.

Some modifications are considered in the equations and used for objects in the process of reentering the Earth. For values for the perigee between 98 km and 156 km, the value of the constant ϵ is 1.01222928. So, it is possible to rewrite,

$$\epsilon^* = a'_o(1 - e) - \epsilon + a_e. \quad (20)$$

The value of ϵ is changed again, when the perigee is below 98 km,

$$\epsilon^* = \frac{20}{X} + a_e, \quad (21)$$

where X =Earth radii / kilometers = 6378.135.

Considering the changes in the constant ϵ , the term $(q_o - \epsilon)^4$ is replaced by

$$(q_o - \epsilon^*)^4 = \left[[(q_o - \epsilon)^4]^{1/4} + \epsilon - \epsilon^* \right]^4, \quad (22)$$

where q_o is a parameter for the SGP4 density function.

The terms used in Eqs. 7 to 17, θ , ϱ , β , η , C_2 , C_1 , C_3 , C_4 , C_5 , D_2 , D_3 and D_4 are described in [1], with the appropriate values of ϵ and $(q_o - \epsilon)^4$.

In the next section, the orbital motions of space debris are studied.

3 Reentry in the Earth

In this section, the orbital motions of space debris are analyzed. The objects, in the process of reentry, are faster when near the Earth's surface. The space debris FENGYUN 30158 has a prediction of reentry for May/2018.

Figures 2 a) and 2 b) show the time behavior of semimajor axis and the time behavior of eccentricity, respectively, of space debris Fengyun 30158. In some months, the process of reentry is completed, when the object reaching the Earth's surface, considering the Earth's radius.

Figures 3 a) and 3 b) show the time behavior of semimajor axis and the time behavior of eccentricity, respectively, of space debris Techedsat 6 43026. In some months, the process of reentry is completed in May 22, 2018.

Table 1 shows some objects in process of reentry. The space debris analyzed can be fragments, tools, rocket bodies from space missions ISS - International Space Station, IRIDIUM 33 and DELTA 1. The predictions are for 2018 and 2019 and they can represent a safety planning and avoid risks to the population that collisions with the Earth can generate.

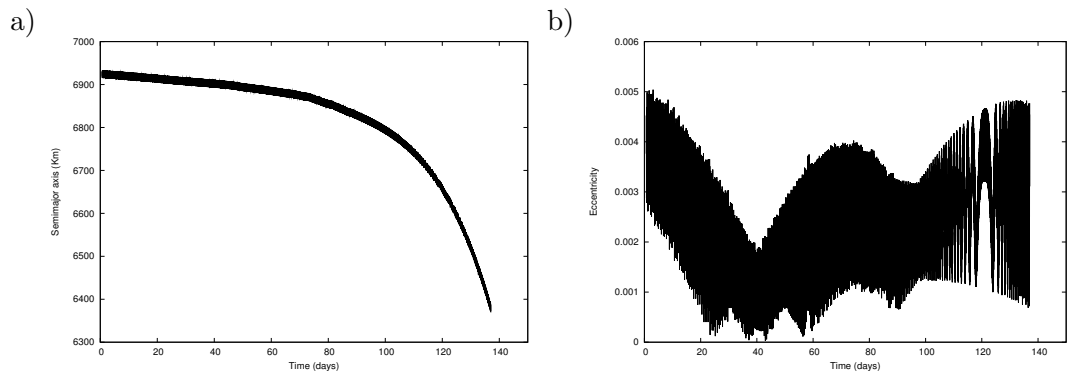


Figure 2: Orbital motion of space debris FENGYUN 30158 corresponding to January/01/2018 to May/18/2018: a) Time evolution of the semimajor axis and b) Time evolution of the eccentricity.

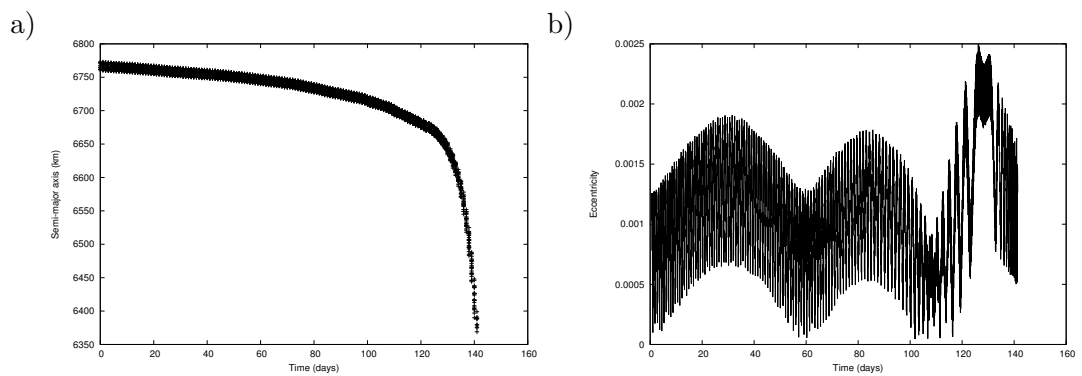


Figure 3: Orbital motion of space debris Techedsat 6 43026 corresponding to January/01/2018 to May/22/2018: a) Time evolution of the semimajor axis and b) Time evolution of the eccentricity.

Table 1: Space debris in process of reentry

Name	Cataloged number	Reentry prediction
ISS deb	43206	November 16, 2018
IRIDIUM 33 deb	33964	May 29, 2018
DELTA 1 deb	00399	September 04, 2019

4 Conclusions

In this work, the orbital dynamics of space debris are studied. There are several operational artificial satellites in Low Earth Orbits, in the same region of most of the space debris orbiting the planet. So, several studies are important to preserve the operability

of the space station, considering the increasing number of distinct objects in the space environment offering collision risks and, consequently, possible lost of mission.

The orbital motion of objects are propagated, considering perturbations of geopotential and atmospheric drag. Real data from the Two Line Elements Set of the NORAD are used as initial conditions to the time evolution of the orbital elements.

The process of reentry of Fengyun 30158 and Techedsat 6 43026 in the Earth are observed when the time behavior of the semi-major axis of the space debris are studied.

One can observe that the collision risk of space debris with artificial satellites and the Planet is growing and solutions for the space debris mitigation are necessary.

As a future work, strategies to reduce space debris in LEO region can be studied.

Acknowledgements

This work was accomplished with support of the CNPQ - Brazil (contract 420674/2016-0), FAPESB (Process 1430/2017) and IFBA.

References

- [1] F. R. Hoots, R. L. Roehrich, Models for Propagation of NORAD Element Sets, *Space-track Report*, 3, 1980.
- [2] R. Osiander, P. Ostdiek, Introduction to Space Debris, *Handbook of Space Engineering, Archeology and Heritage*, 2009.
- [3] J. C. Sampaio, E. Wnuk, R. Vilhena de Moraes, S. S. Fernandes, Resonant Orbital Dynamics in LEO Region: Space Debris in Focus, *Mathematical Problems in Engineering (Print)*, pags. 1-12, 2014.
- [4] J. C. Sampaio, R. Vilhena de Moraes, S. S. Fernandes, Resonant Orbital Dynamics of CBERS Satellites, In: *Proceeding Series of the Brazilian Society of Computational and Applied Mathematics*, v. 4, n. 1, 2016.
- [5] Space Track. Archives of the 2-lines elements of NORAD. Available at: <www.space-track.org>, accessed in January, 2018.